6 Magnetic domains near the spin-reorientation transition

The modification of magnetic domains and domain walls at the continuous spiral-like spin-reorientation transition of ultrathin Ni/Cu(100) films at 300 K as a function of film thickness is discussed in section 6.1. In section 6.2 the reorientation of the magnetization of Fe/Ni bilayers on Cu(100) from the out-of-plane direction to an in-plane direction is analyzed as a function of the Fe layers thickness at room temperature. The orientation of the individual magnetizations of the Fe and the Ni layer is determined element-selectively as a function of the thickness. Finally, the change of the effective magnetic anisotropy and the value of the magnetic moments at the Fe-Ni interface is discussed.

6.1 Continuous reorientation of the magnetization in Ni/Cu(100) films

The formation of in-plane magnetized domains in the thickness range of 5 ML to 8 ML Ni/Cu(100) has already been discussed in section 5.1. It was found that the domain structure remains unchanged for Ni thicknesses below 9.5 ML. Around 9.5 ML a spontaneous modification of the domain wall is observed, whereby about 0.5 μm wide protrusions of approximately 6 μm length, along with a reduced magnetic contrast, are formed perpendicular to the domain wall as shown in Fig. 6.1 (b). These features correspond to an elongation of the domain wall within the 10 μm-field of view of 180%. The reduced MC indicates a change of the magnetization direction within the protrusions. Moreover, smaller domains of inverse magnetic contrast emerge within the still existing and large in-plane magnetized original domains. This also corresponds to an elongation of domain boundaries, which can be understood in terms of the lowered domain wall energy density per unit length γ due to the reduced effective anisotropy at the spin-reorientation transition according to $\gamma = d\sqrt{A\,K_2^{\text{eff}}}$, d being the film thickness. The reduction of the effective anisotropy is correlated with a domain wall broadening according to $w = 2\sqrt{A/K_2^{\text{eff}}}$. A typical example is shown in Fig. 6.2 by two domain wall profiles obtained from the two line scans (I) and (II) in image (c) of Fig. 6.1. While the width of the domain wall measured at (I) is comparable to the typical wall width of fully in-plane magnetized ultrathin

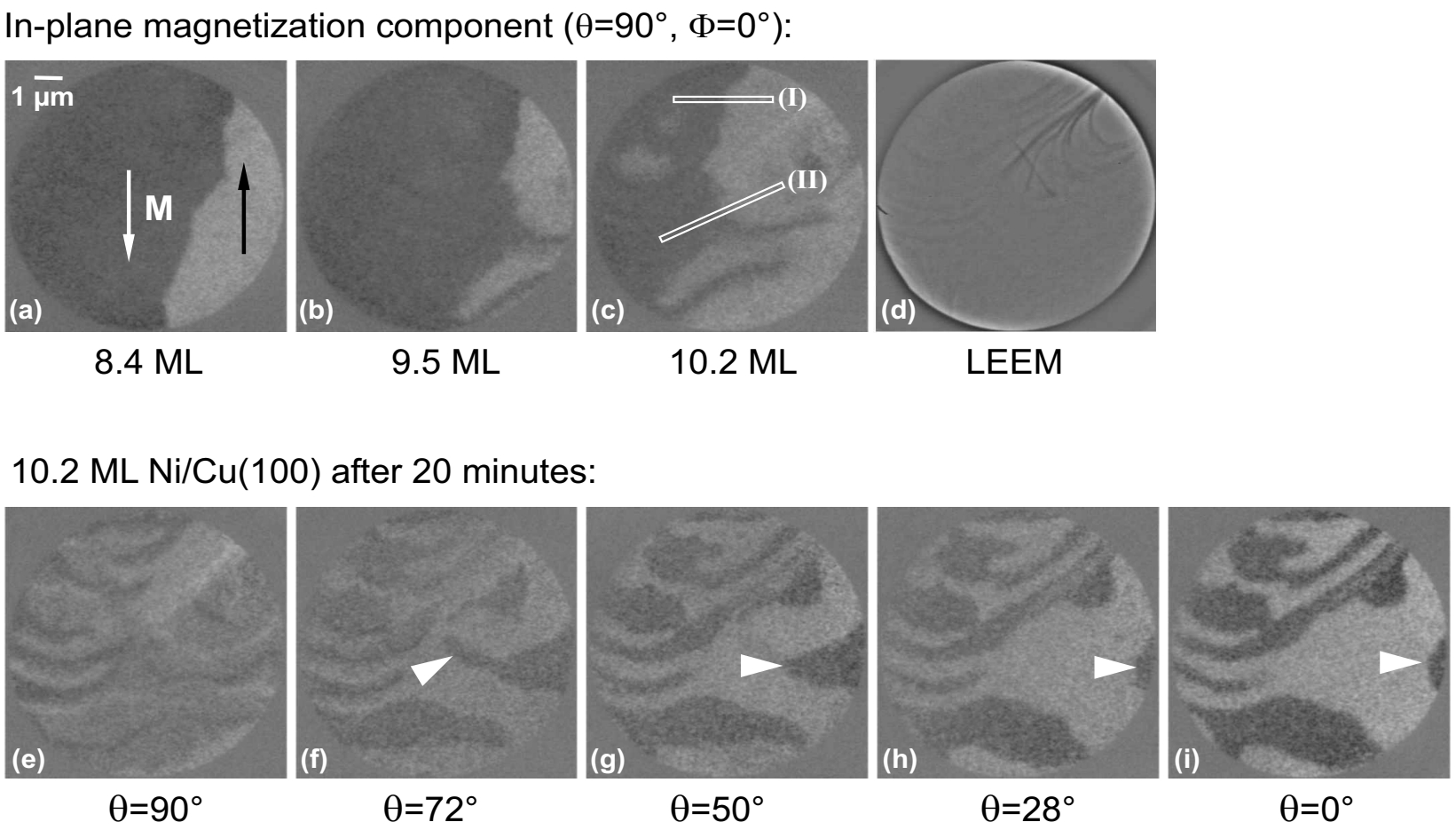

Figure 6.1: Spin-reorientation transition of Ni/Cu(100) at 300 K as a function of the thickness. The domain wall of the 8.4 ML in-plane magnetized Ni film (a) spontaneously forms elongated protrusions normal to the wall as the SRT thickness of $d_c = 9.5$ ML is reached (b). At 10.2 ML smaller domains of a reversed magnetization direction appear within the original domains (c). The domain wall in (c) was centered manually, and the profiles (I) and (II) are shown in Fig. 6.2. 20 min after film deposition. The 10.2 ML Ni film reveals a multi domain pattern with the magnetizations canting in an orientation close to the surface normal as indicated by polar angular investigations (e)-(i).

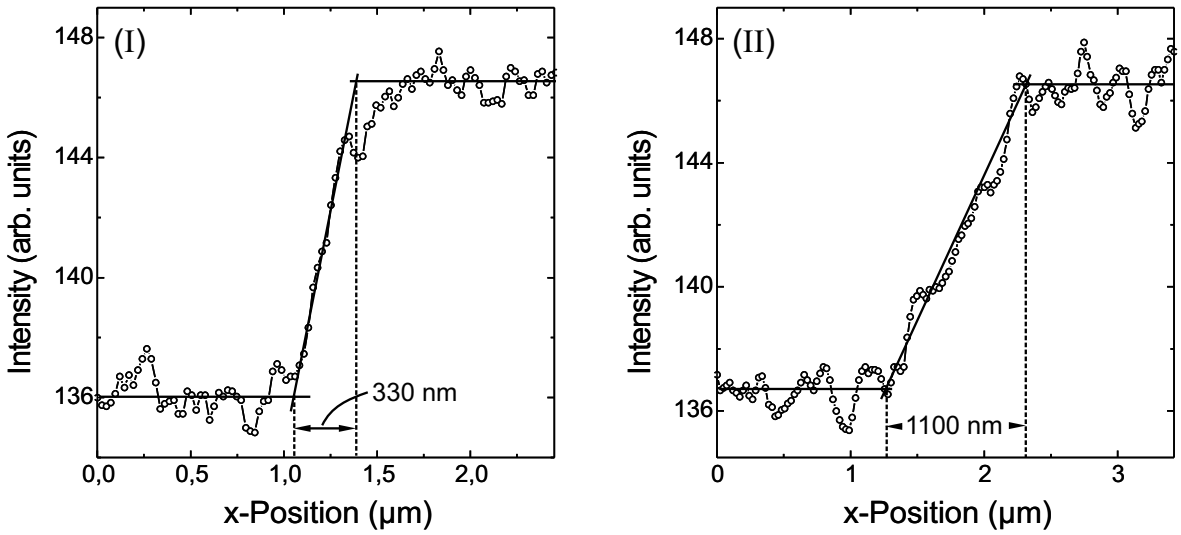

Figure 6.2: Domain wall profiles taken at the sites (I) and (II) of the domain image (c) in Fig. 6.1 of a 10.2 ML Ni/Cu(100) film at the SRT. While the width of the upper part of the domain wall (I) is still comparable to the typical wall width of fully in-plane magnetized ultrathin Ni/Cu(100) films ($300 - 400$ nm), the width of the wall segment (II), in close vicinity to the wall protrusion, is increased by ≈300% due to the lowered effective anisotropy at the SRT according to $w = 2\sqrt{A/K_2^{\text{eff}}}$.

Ni/Cu(100) films ($300 - 400$ nm), the width of the wall segment (II), which is located in close vicinity to the wall protrusion, is increased by ≈300%. Similar results are obtained for wall segments of the elongated protrusion and also for the smaller domains with inverse magnetic contrast (bright areas). Here, the width of the walls ranges from 500 nm to more than 1200 nm. The determination of the exact domain wall width, however, is more difficult here since the signal to noise ratio decreases, due to the decrease of MC in these areas.

The time evolution of the domain configuration of the 10.2 ML Ni/Cu(100) film was checked by polar angular investigations 20 minutes after completion of the film growth. Fig. 6.1 (e) demonstrates that a meandering domain pattern with a low magnetic contrast of the in-plane component of the magnetization $\mathbf{M}$ has formed. As the polar angle of the polarization $\mathbf{P}$ was successively lowered to $\theta = 0°$, where $\mathbf{P}$ is aligned perpendicular to the surface, the MC increased, which is shown in Fig. 6.1 (e)-(i). The strongest MC in (i) indicates that the component of $\mathbf{M}$ perpendicular to the surface is largest, which means that $\mathbf{M}$ is oriented largely parallel to the surface normal. The reduction in size of the dark imaged domain at the right hand side of the SPLEEM images (see arrow) is not an angular dependent effect, but it corresponds to an increase in size of the respective surrounding out-of-plane magnetized domain as a function of time. This was checked by subsequently increasing the polar angle of $\mathbf{P}$ back to $\theta = 90°$. It was found (not shown here), that the meandering domain structure further developed to larger domains as a function of time. After 60 minutes waiting time at a base pressure of 2×10^{-8}

Pa, which corresponds to a gas exposure of 0.54 Langmuir, the orientation of $\mathbf{M}$ of the 10.2 ML Ni/Cu(100) film was perpendicular to the film surface. This indicates the completion of the spin-reorientation transition. The adsorption of O and CO at the Ni surface is known to reduce the surface anisotropy and therefore shifts the SRT to lower thickness values [83,96,97]. We would like to emphasize, that although the SRT as a function of the Ni layer thickness was not completed at 10.2 ML, as confirmed by the existence of a magnetization component within the film plane (Fig. 6.1 (c) and (e)), the magnetization vector further on rotates completely out-of-plane. This is due to the fact that the surface anisotropy $2K_2^S$ is reduced, such that the positive volume anisotropy K_2^V becomes the dominant contribution to the total anisotropy.

In order to determine the orientation of the magnetization during the SRT, angular dependent domain imaging has been performed. Therefore, the perpendicular and two orthogonal in-plane directions of $\mathbf{M}$ have been probed. The results of these additional measurements, which have been done by C. Klein and A. K. Schmid [191] recently, are depicted in Fig. 6.3. No perpendicular component of $\mathbf{M}$ is detected in the thickness range $5 - 9$ ML (a_1). The analysis of the clear magnetic contrast in the $\Phi = -162^\circ$ in-plane orientation of $\mathbf{P}$ and the weak inverse MC in the $\Phi = -72^\circ$ in-plane orientation reveals, that the magnetization vector is aligned along the $\Phi = -176^\circ \pm 5^\circ$ within the film plane. Comparing this direction of $\mathbf{M}$ with the LEEM and the LEED images presented at the bottom of Fig. 6.3 indicates, that the easy axis of the magnetization is collinear to the parallel alignment of the Cu step edges which do not run along the $\langle 011 \rangle$ directions, which are known to be low energy step directions on Cu surface vicinal to [100], Ref. [192]. Moreover, $\langle 011 \rangle$ is known to be the easy in-plane orientation for Ni/Cu(100). This means, that the in-plane easy axis of the magnetization of ultrathin Ni/Cu(100) films is predominantly determined by a step induced uniaxial anisotropy if many steps are aligned parallel. In the present case this step induced anisotropy overcomes the magnetocrystalline anisotropy along $\langle 011 \rangle$. In previous studies on the influence of parallel Cu step edges on the easy in-plane direction of the magnetization in Ni/Cu(001) it was shown, that the step induced anisotropy in films grown on Cu(001) crystals with miscuts of $<1^\circ$ [10] and 2.5° [90] orients the magnetization parallel to the steps.

At the start of the SRT around 9.3 ML a breakup into a state of micrometer-sized domains of irregularly shaped protrusions and isolated areas of a changed orientation of the magnetization with respect to the surrounding domain takes place. At the same time the magnetization rotates out of the film plane by an angle $\theta = 23^\circ \pm 5^\circ$ with respect to the sample's normal within the bright domain in (a_2). This angle is determined from the magnetic contrast of the three SPLEEM images at 9.3 ML. Here, both in-plane directions of $\mathbf{P}$ yield a similar MC within the domain, which has formed in the upper left of the images, indicating that the in-plane component of $\mathbf{M}$ has changed (b_3, b_4). The deviation in the domain shape of the images showing the in-plane component of $\mathbf{M}$ (b_3, b_4) from the domain pattern in (a_2), i. e. the perpendicular component,

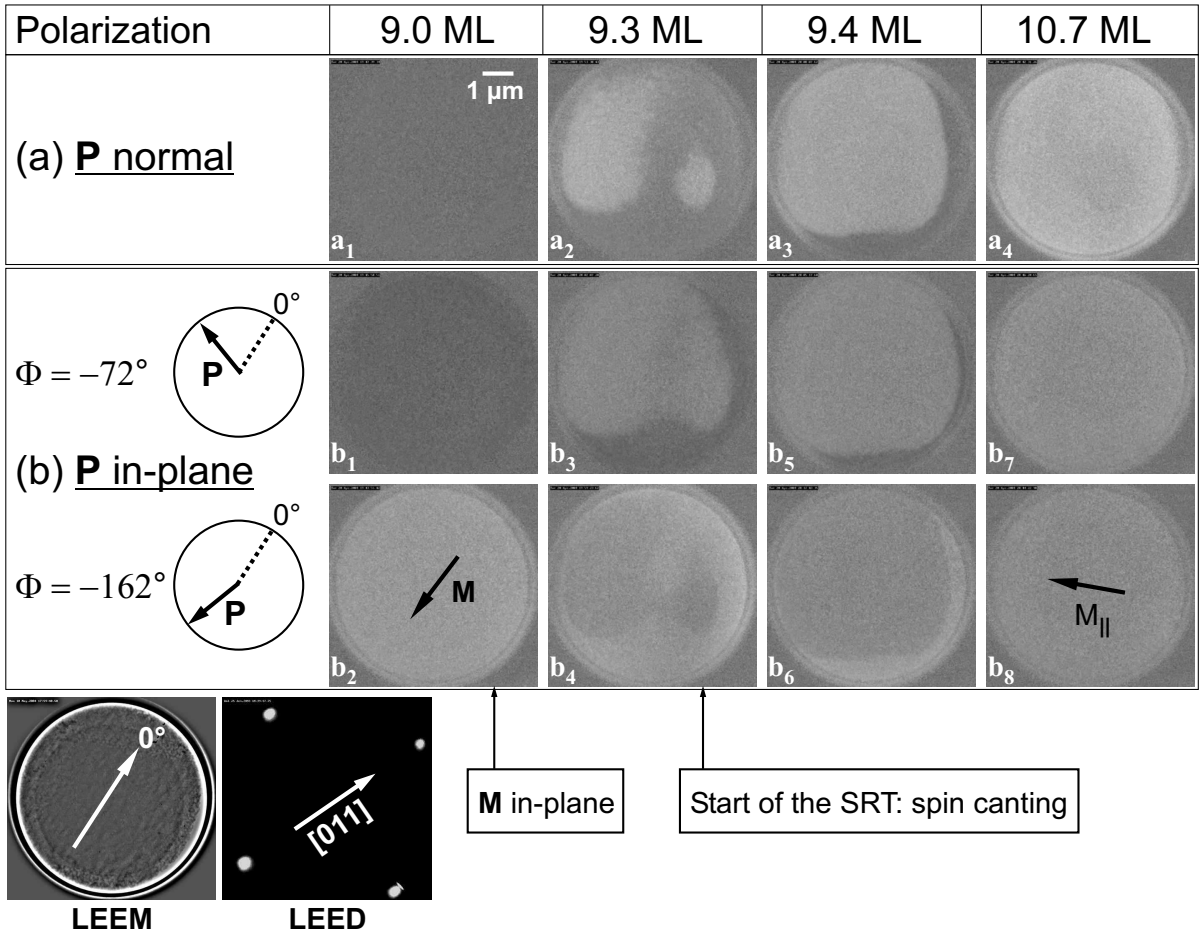

Figure 6.3: Spin canting at the SRT of Ni/Cu(100) as a function of the thickness at 300 K. At 9.0 ML the magnetization lies in the film plane pointing into the $\Phi = -176°$ direction (a_1, b_1, b_2), which is rather parallel to the Cu step edges than parallel to the [011] direction, as indicated by the LEED image (taken at 150 eV). The continuous SRT takes place via the formation of micrometer-sized domains of irregular shape (a_2, b_3, b_4). At 10.7 ML an out-of-plane magnetized domain larger than the field of view (7 μm) has formed. The canted magnetization vector at 10.7 ML is characterized by the polar angle $\theta \approx 23°$ and the azimuthal angle $\Phi \approx -113°$.

is due to the domain evolution process, since the images could not be imaged at the same time. However, the canting of the magnetization is clearly visible in the image series at 9.3 ML Ni/Cu(100). As the Ni layer thickness is further increased up to 10.7 ML, the canting angle θ remains almost constant, while the domain size increases beyond the field of view (7 μm) where the in-plane component of $\mathbf{M}$ has rotated to $\Phi = -113° \pm 5°$. Finally, the magnetization is perpendicular to the surface, as the Ni thickness exceeds 11 ML (not shown). In conclusion, the rotation of the in-plane component of $\mathbf{M}$ proceeds from a parallel alignment to the steps to an orientation perpendicular to the steps. The superposition of this rotation and the reorientation of the magnetization toward the surface normal results in a *spiral-like* motion of $\mathbf{M}$ during the SRT. Such spiral-like SRT was also observed by Dhesi *et al.* [90] and Jähnke *et al.* [10].

6.2 Spin-reorientation transition of Fe/Ni bilayers on Cu(100)

The magnetic domain microstructure of 0 to 3 ML of Fe on 7 and 11 ML Ni/Cu(100) films was studied by SPLEEM at 300 K. As described in chapter 5.3.1 the two Ni underlayers vary in their anisotropy due to the different layer thickness. The 7 ML Ni/Cu(100) film was in a canted magnetization state, whereas the 11 ML Ni/Cu(100) film was perpendicularly magnetized due to the large positive volume anisotropy. However, qualitatively, the spin-reorientation transition was found to be similar for Fe/Ni bilayers fabricated on a 7 ML and an 11 ML Ni underlayer. In both cases we have observed a continuous spiral-like SRT, accompanied by a stripe domain state. In section 6.2.1 the ferromagnetic coupling between the Fe and Ni layer is investigated by means of angular dependent XMCD measurements. The nature of the continuous SRT in Fe/Ni/Cu(100) films is discussed in detail in the following sections, including the role of magnetic moments at the Fe/Ni interface determined by XMCD.

6.2.1 Coupling between Fe and Ni layers

SPLEEM is not an element-selective technique. The magnetic contrast of Fe/Ni bilayers on Cu(100) arises from the magnetization of both the Fe and the Ni layer, since below an energy of the electrons of 10 eV, the penetration depth of the spin-polarized beam may be several nanometers. No domains or domain walls of different magnetic contrast are observed, which would otherwise indicate a different position of domains or their magnetization orientation in the Ni underlayer with respect to the Fe layer. Thus, there is evidence for a strong ferromagnetic coupling between the Ni and the Fe layer. In order to confirm this coupling, angular dependent element-specific XMCD measurements have been performed. The orientation of the magnetization of both layers was found to be parallel in the whole thickness range studied, indicating a ferromagnetic coupling of out-of-plane and in-plane magnetized Fe/Ni bilayers. Since the helicity of the x-rays was kept constant at $\sigma = -1$, and the magnetization was switched by 180° to obtain the two individual (Fe, Ni) XMCD spectra, a ferromagnetic coupling is revealed, if the algebraic sign of the intensities equals, as obtained from the L_2 (L_3) edges of the spectra for Fe and Ni, respectively. An inverse sign would otherwise identify an antiferromagnetic coupling. Fig. 6.4 typically shows the ferromagnetic coupling of an Fe_4/Ni_{17}/Cu(100) film as obtained from XMCD spectra.

The analysis of the angular dependence of the data, which have been corrected in respect of saturation effects, is consistent with the expected $\cos\theta$-law [153]. This indicates that the bilayer is perpendicularly magnetized, and it does not reveal a canted magnetization. At an Fe thickness of 6.5 ML the magnetization of the bilayer has rotated into the film plane. The parallel alignment of the magnetizations within the plane of the Ni and the Fe layer is demonstrated

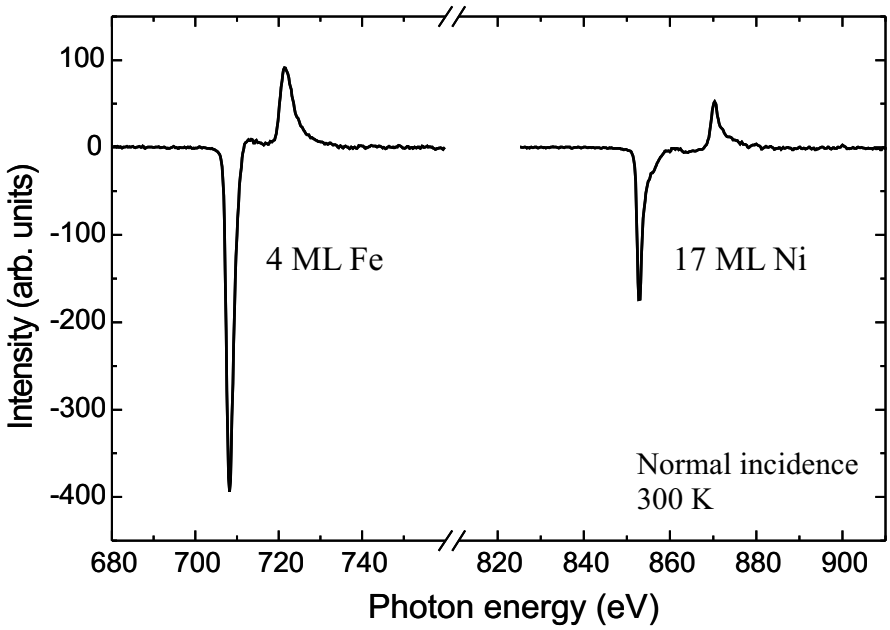

Figure 6.4: Element-selective XMCD signals of a perpendicularly magnetized Fe_4/Ni_{17}/Cu(100) film at the Fe and Ni $L_{2,3}$ edges at normal photon incidence ($\theta = 0°$). The equal sign of the intensities at the corresponding L-edges of Fe and Ni reveals the ferromagnetic coupling between both layers.

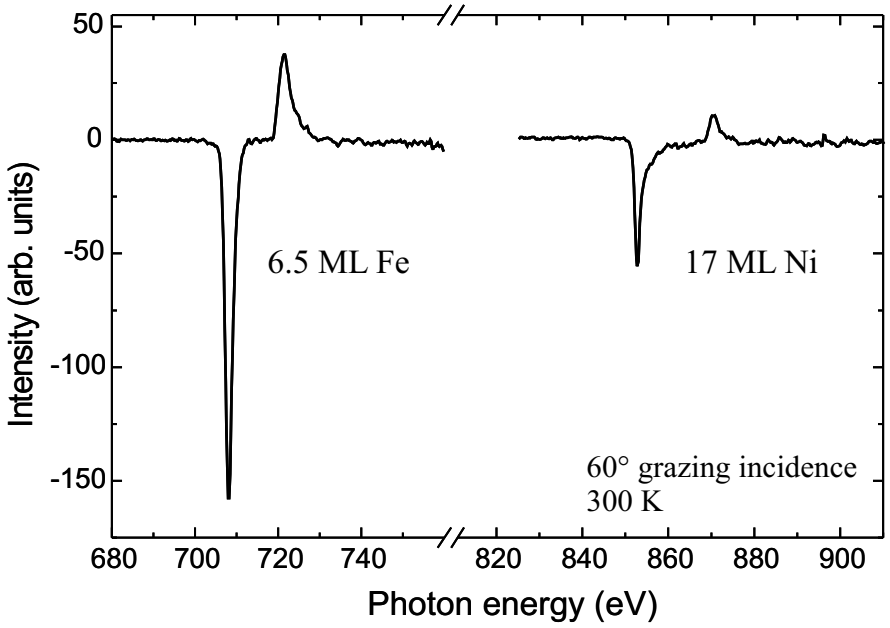

Figure 6.5: Element-selective XMCD signals of an in-plane magnetized $Fe_{6.5}/Ni_{17}$/Cu(100) film at the Fe and Ni $L_{2,3}$ edges at a grazing photon incidence of $\theta = 60°$ with respect to the sample's normal. The equal sign of the intensities at the corresponding L-edges of Fe and Ni indicates the ferromagnetic coupling between both layers.

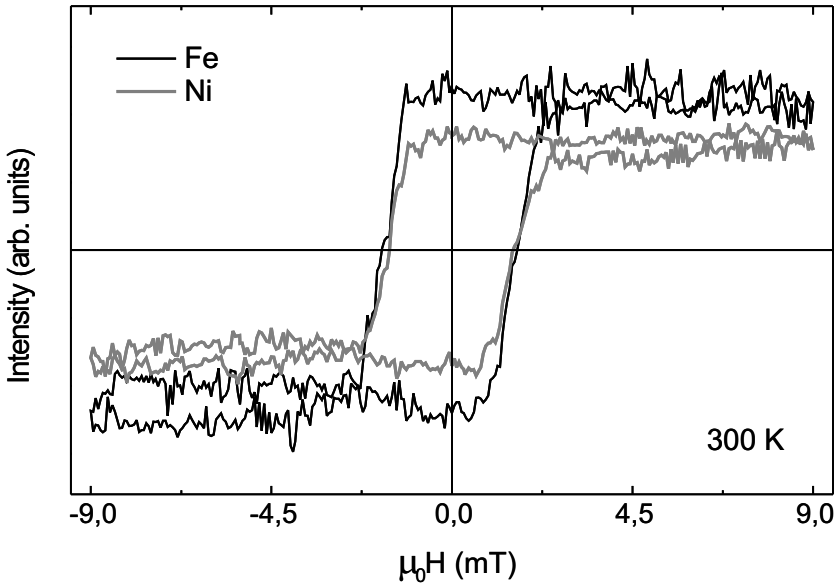

Figure 6.6: Element-selective hysteresis loops taken at the L_3 edges of Fe and Ni of an Fe_{17}/Ni_{17}/Cu(100) film at a grazing angle of incidence of $\theta = 80°$. Both loops show the same magnetization switching as the external field is reversed indicating the ferromagnetic coupling. The rectangular shape exhibits the easy axes of the magnetization lying in the plane, and the equal coercive field (± 1.6 mT) confirms the strong coupling. The data are smoothed and have been corrected in respect of a linear background signal.

in Fig. 6.5, which shows the XMCD spectra at a grazing angle of $\theta = 60°$ with respect to the sample's normal. No dichroism was observed at normal incidence. Again, the negative (positive) intensity values at the L_3 (L_2) edges of Fe and Ni, respectively, confirm the ferromagnetic coupling in the bilayer. Moreover, the coupling was determined, by recording element-specific hysteresis loops. At a grazing angle of $\theta = 80°$ the reflected x-ray was detected by a photodiode, which gives rise to an output voltage proportional to the magnetization. The energy of the x-ray was set to 708 eV and 852 eV, respectively, which corresponds to the L_3 edges of Fe and Ni. Magnetic fields up to ± 9 mT [1] were applied in-plane during the magnetization reversal, using a water-cooled pair of Helmholtz coils. Both hysteresis loops, which have been smoothed and corrected by subtracting a linear background signal, are depicted in Fig. 6.6. Despite the electronic noise of the measurements the hysteresis loops for Fe and Ni clearly show the same magnetization switching as the external field is reversed. The almost rectangular shape of both loops indicates that the easy axis of the magnetization lies in the film plane. A strong ferromagnetic coupling between both layers is revealed by the equal coercive field of 1.6 mT.

[1] The magnetic field is here given in the SI unit Telsa of the magnetic induction $\mu_0 H$

6.2.2 Magnetic moments per Fe and Ni atom

Exploiting the element-selectivity of the XMCD method the magnetic moments per Fe and Ni atom have been determined for out-of-plane magnetized Fe/Ni bilayers as a function of the Fe layer thickness at 300 K. This was done in order to study the effect of alloying at the Fe/Ni interface on the magnetic moments per atom. The results for Ni and Fe are listed in table 6.1 and 6.2, respectively. The orbital magnetic moment μ_L and the spin magnetic moment μ_S are derived following the approach of [154]. Since the number of $3d$-holes n_h enters the equations to determine μ_L and μ_S (see section 2.2.1), a difficulty arises at the Fe/Ni interface, where the number of holes for Ni and Fe will change with the degree of intermixing which is not known. Recent calculations of the individual density of states (DOS) of Fe and Ni in variously composed Fe-Ni alloys [193] revealed, that the number of $3d$-holes in the minority band of Fe increases drastically with increasing Fe amount due to a broadening of the DOS above the Fermi level. The same effect –but much less pronounced– is found for the majority band. The inverse behavior is calculated for Ni: a narrowing of the DOS leads to a reduction of n_h^{Ni}. Experimentally, the number of holes can be deduced from the alloy-dependent change of the integrated isotropic absorption spectra (half-sum spectra), which are proportional to n_h. The detailed analysis of the area of the normalized isotropic absorption spectra of Ni reveals a linear decrease with increasing Fe layer thickness (not shown here). Based on the above mentioned theoretical findings we attribute this decrease to a reduction of $3d$-holes of Ni and not due to an absorption effect by the Fe cap layers. The validity of this assumption is confirmed by the increasing value of the integrated half-sum spectra of Fe with increasing Fe layer thickness. For the 17 ML Ni/Cu(100) film $n_h^{\mathrm{Ni}} = 1.5$ has been used, which is in close agreement to theoretical values [151,194] and was found experimentally for a 23 ML Ni/Cu(100) [195]. From the linear decrease of the Ni L_3 edge of the isotropic spectra versus the Fe layer thickness the number of Ni $3d$ holes is determined to be $n_h^{\mathrm{Ni}} = 1.36$ for the Fe_1/Ni_{17} film and $n_h^{\mathrm{Ni}} = 1.23$ for the Fe_4/Ni_{17} film. According to the decrease of n_h^{Ni} the respective residual number of holes have been added to $n_h^{\mathrm{Fe}} = 3.4$ which is the number of $3d$-holes of Fe taken from Ref. [196].

The magnetic moments of Ni in Fe/Ni/Cu(100) films of various Fe thicknesses listed in table 6.1 can be considered as constant and in reasonable agreement with previous measurements of a 15 ML Ni/Cu(100) film [197] within the error bar of $\pm 0.05\ \mu_{\mathrm{B}}$. Since from XMCD the averaged element-selective moment of a film is obtained and the changes of moments at the interface contribute to the moment of the whole film of 17 ML thickness, only minor changes of the total moment may be expected. The ratios μ_L/μ_S, however, are larger than determined generally for Ni/Cu(100) films in that thickness range. It should be noted that the relatively large error bar arises from the average of only two measurements. To obtain more reliable data five spectra should be averaged.

By considering the magnetic moments of 1 ML and 4 ML Fe of the same Fe/Ni bilayer,

Table 6.1: Magnetic moments per Ni atom of an $Fe_x/Ni_{17}/Cu(100)$ film as a function of the Fe layer thickness x.

Fe thickness (ML)	$\mu_L(\mu_B)$	$\mu_S(\mu_B)$	$\mu_{tot}(\mu_B)$	$\frac{\mu_L}{\mu_S}$
0	0.13	0.60	0.73	0.22
1.0	0.12	0.60	0.72	0.21
4.0	0.12	0.65	0.77	0.18
15 ML Ni/Cu(100) [197]	0.08	0.61	0.69	0.13

Table 6.2: Magnetic moments per Fe atom of an $Fe_x/Ni_{17}/Cu(100)$ film as a function of the Fe layer thickness x.

Fe thickness (ML)	$\mu_L(\mu_B)$	$\mu_S(\mu_B)$	$\mu_{tot}(\mu_B)$	$\frac{\mu_L}{\mu_S}$
1.0	0.22	1.47	1.68	0.15
4.0	0.28	2.05	2.36	0.14
3.8 ML Fe/Cu(100) [198]	0.25	3.46	3.71	0.07

good agreement is found for the orbital magnetic moment with previous measurements of a 3.8 ML Fe/Cu(100) film [198]. The spin magnetic moment of 1 ML Fe is determined to be 30% smaller than the bulk value of bcc Fe. In order to clarify if the spin moment of 1 ML Fe is reduced, measurements at low temperatures are required which have not been performed. On the other hand the Fe monolayer is deposited on perpendicularly magnetized Ni, which due to the direct exchange interaction stabilizes the magnetic moments of Fe against thermal fluctuations and should yield a magnetic moment of Fe near the low temperature value. The formation of an Fe-Ni alloy leads to an average magnetic moment of $\approx$1.6 μ_B of the alloy according to the Slater-Pauling curve, if an $Fe_{0.5}Ni_{0.5}$ alloy with fcc structure is assumed at the interface as discussed in section 1.1.2. The individual magnetic moments per Fe and Ni atom, which correspond to that average value, have been determined by neutron diffraction experiments to be $\mu^{Ni} \approx 0.7\ \mu_B$ and $\mu^{Fe} \approx 2.5\ \mu_B$ [46] which in the case of Fe is contradictory to our measurement.

The total magnetic moment of 4 ML Fe on 17 ML Ni/Cu(100) is determined to be $2.36 \pm 0.05\ \mu_B$. In order to obtain the contribution of the three additional Fe layers of the 4 ML film compared to the monoatomic Fe layer at the Fe-Ni interface, the following approach is considered. Assuming an $Fe_{0.5}Ni_{0.5}$ alloy at the interface, three different Fe layers contribute to the measured moment of Fe: the Fe interface layer with a magnetic moment equal to that of 1 ML Fe on Ni/Cu(100) and full coordination number, the interior double layer and the surface layer with a reduced coordination number. The average magnetic moment μ of the three topmost

layers is then given by $\frac{1}{4} \times 1.68\ \mu_B + \frac{3}{4} \times \mu\ \mu_B = 2.36\ \mu_B$, which reveals $\mu = 2.59\ \mu_B$. This value indicates a high-spin state of Fe and gives strong evidence for the fct or fcc structure. Moreover, this result becomes important in terms of interpreting the SRT, which is discussed in the following sections in detail, since a high-spin state of Fe gives rise to a large shape anisotropy that favors an in-plane orientation of the magnetization.

6.2.3 Continuous SRT as a function of the Fe layer thickness

The spin-reorientation transition of Fe/Ni bilayers on Cu(100) has been investigated as a function of the Fe layer thickness in the range of 0 to 3 ML Fe at room temperature. At first, the magnetization state of an 11 ML Ni/Cu(100) film was magnetically characterized by SPLEEM, by probing the three components of the magnetization. The perpendicular orientation of the magnetization of the 11 ML Ni/Cu(100) film was confirmed by imaging the magnetic domain structure of the film in the perpendicular and in several in-plane orientations of the electron beam polarization $\mathbf{P}$ as shown in Fig. 6.7 ("0 ML Fe"). The magnetic domain pattern of the Ni film consists of stripes of several micrometers width with a perpendicularly up and down oriented magnetization ([100] direction) as depicted in (a_1). No in-plane magnetization components were found in this pure Ni film. Typically, the two images in the left most column ("0 ML Fe") in Fig. 6.7 (b) were acquired with a spin-polarization oriented along two orthogonal in-plane directions at $\Phi = -4°$ and $\Phi = -94°$. The absence of magnetic contrast in these images confirms that there is no spin canting in the Ni/Cu(100) film of 11 ML thickness. Upon Fe deposition on top of the Ni/Cu(100) film, the modification of both the domain pattern and the magnetization direction is demonstrated by the sequence of images illustrated in Fig. 6.7. The deposition of less than 1 ML Fe results in an increase of the magnetic contrast along the perpendicular direction and a slight broadening of the Ni domain pattern as described in section 5.3.1. Upon further Fe deposition the out-of-plane MC (Fig. 6.7 (a)) increases up to 2.5 ML Fe. Here, the onset of the formation of narrower domains is observed, which corresponds to the start of the SRT. As the Fe layer thickness is further increased, the large out-of-plane domains breakup into ≈180 nm wide stripe domains. The correlation of the shape of the magnetic domains with the topography of the Cu crystal is revealed by the LEEM image of the bare Cu surface, which is shown in the lower left of Fig. 6.7. The domain walls of the stripe domains are obviously aligned parallel to the Cu atomic steps. A typical profile of the stripe domain pattern at the maximum number of stripes, i. e. at 2.6 ML Fe, is depicted in Fig. 6.8. Mostly cosine-shaped profiles of the stripe domains similar to that of 2.2 ML Fe/Cu(100) are revealed. In contrast to the calculated perpendicular orientation of the magnetization within the stripe domain pattern of cosine-like profile by Jensen *et al.*, the magnetization is canted within the narrow stripe domains. The different amplitudes in the figure indicate different canting angles of the magnetization within the respective stripe domains.

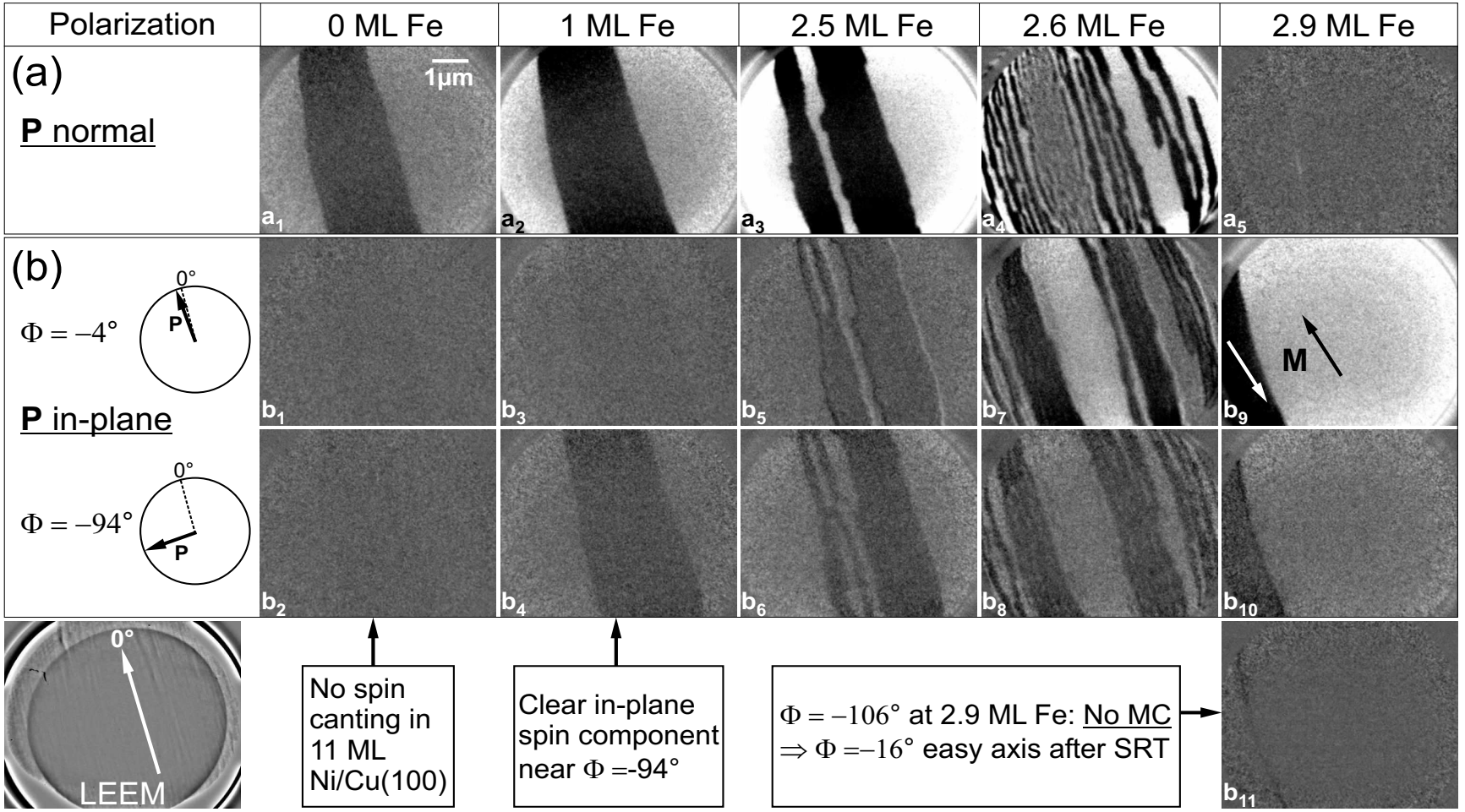

Figure 6.7: Spin-reorientation transition of an Fe_x/Ni_{11} bilayer on Cu(100) at 300 K as a function of the Fe layer thickness ($x = 0 - 2.9$ ML). The SRT takes place by a continuous spin rotation, a breakup of domains into stripe domains parallel to the Cu step edges and a reformation to large in-plane magnetized domains at 2.9 ML Fe, where the out-of-plane magnetic contrast has vanished (a_5). For details see text.

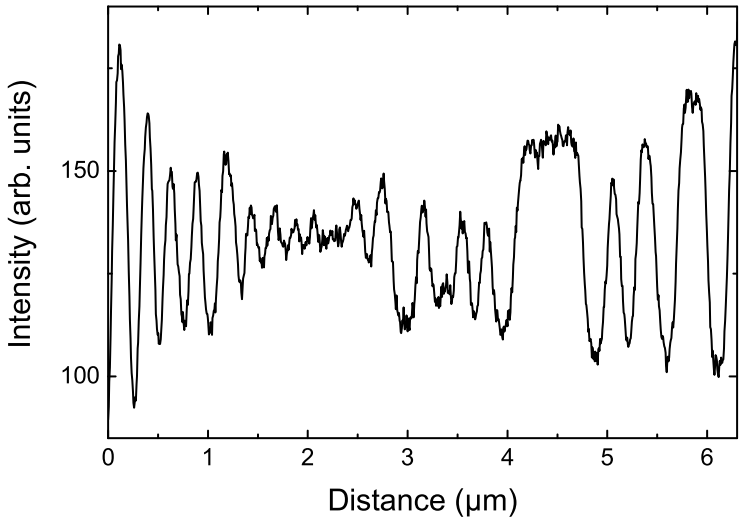

Figure 6.8: Profile of the stripe domain pattern of an $Fe_{2.6}/Ni_{11}/Cu(100)$ film probing the magnetization component perpendicular to the film surface. The different amplitudes are due to different canting angles of the magnetization within the respective stripes.

Finally, the MC in perpendicular orientation vanishes at 2.9 ML Fe. This proves that the magnetization is now completely oriented in the film plane. Unlike this finding, a perpendicular orientation of the magnetization was reported for Fe coverages up to 11 ML on 15 ML Ni/Cu(100) by O'Brien *et al.* using XMCD [25]. Thereby, around 4 ML Fe a transformation from the fct to the fcc structure of Fe occurred, and the small detected perpendicularly oriented magnetization of the Fe film was attributed to the Fe layer at the Fe/Ni interface. An in-plane oriented magnetization was found by these authors for an Fe film thickness larger than 11 ML, i. e. a similar behavior as observed for Fe/Cu(100) films.

In order to determine the easy axis of the in-plane magnetized domains at 2.9 ML Fe, the electron beam polarization $\mathbf{P}$ was rotated, until the MC between the domains vanished. Since the MC vanishes at $\Phi = -106°$ (see b_{11}), the magnetization orientation within the domains lies perpendicular to this angle, i. e., the magnetization within the domains is parallel and antiparallel at an angle of $\Phi = -16°$ with respect to the step edges, as indicated by the arrows in the image (b_9). No magnetization orientation at 90° with respect to this direction was found, as one might have expected for a cubic system. The image contrast at $\Phi = -106°$ vanishes and reveals a 300 nm wide Néel wall, which is visible by the line of darker contrast on the left hand side of this image (b_{11}). Within this wall, the magnetization rotates in the film plane. In the core of the wall the magnetic moments are aligned perpendicular to the easy axis of the domains. A Bloch wall would not cause any magnetic contrast in the middle of the wall for the given $\mathbf{P}$. Since there was no technique available to verify the crystal orientation in the SPLEEM setup at that time, we can only make the following reasonable assumption about the relation of the domain pattern to the crystallographic direction. It is known that the magnetization $\mathbf{M}$ of Ni/Cu(100) films favors the [011] in-plane direction in the thickness range above 6 ML [33], whereas in

Fe/Cu(100) $\mathbf{M}$ favors a [001] in-plane direction with a much larger in-plane anisotropy than for Ni/Cu(100). Therefore, in the coupled Fe/Ni/Cu(100) system the [001] direction most likely is the easy axis. It should be noted, that for one single series of SPLEEM images, which were taken on Fe/Ni films grown on a different Cu(100) crystal a LEED investigation exists. The comparison of the easy axis of the magnetization determined from the domain image of an $Fe_{2.8}/Ni_{7.5}$/Cu(100) film with the corresponding LEED image (Fig. 5.13) confirms the easy axis of the bilayer system to be [001]. As stated already in section 5.3.2, the LEED system was installed after the measurement. However, the crystal orientation was imaged with the Cu(100) substrate being in the same position as for the previously reported domain images. As shown above, the $\Phi = -16^\circ$ direction is the easy axis of the magnetization of the $Fe_{2.9}/Ni_{11}$/Cu(100) film, which according to our interpretation is thus parallel to the [001] crystallographic axis of the bilayer. Based on these reasonable assumptions regarding the orientation of the used crystal, the step edges, which are seen in the LEEM image of Fig. 6.7, have no certain orientation to a crystallographic axis. This indicates that the preferential direction caused by cutting the crystal to a Cu(100) surface has a lower energy than the [011], which is known to be a low energy step direction on Cu surfaces vicinal to [100] (Refs. [90,192]). Note, that the in-plane components $M_{||}^{\uparrow}$ and $M_{||}^{\downarrow}$ of the canted and oppositely oriented domains could not be detected by second harmonic generation [10] or x-ray magnetic circular dichroism [90], since these techniques average over large areas.

The breakup into stripe domains is also observed for the two in-plane directions (Fig.6.7 (b)), which unambiguously shows that the magnetization of the bilayer is canted within the stripes. The canting angle θ with respect to the film normal increases with Fe coverage as seen by the increase of the MC in the series of images on top in Fig. 6.7 (a). Hence, the reorientation of the magnetization from perpendicular to in-plane with increasing Fe layer thickness occurs via a breakup of the original domain pattern and *simultaneously*, by a continuous rotation of $\mathbf{M}$ within the individual domains.

Interestingly, at a coverage of 1 ML Fe, a magnetic contrast appears also for the polarization vector $\mathbf{P}$ at $\Phi = -94^\circ$ as shown in Fig. 6.7 (b) (see b_4). There is nearly no MC for 1 ML Fe if $\mathbf{P}$ is set to $\Phi = -4^\circ$, which is perpendicular to $\mathbf{P}$ in the above described image. At larger coverages of Fe the contrast becomes much stronger for $\mathbf{P}$ along $\Phi = -4^\circ$ but stays constant for $\mathbf{P}$ along $\Phi = -94^\circ$, at least within the error bar of $\pm 5^\circ$, which arise from the uncertainty in determining the angle Φ from the SPLEEM images. The analysis of the grayscale images (normalized to their background, which is the area around the circular field of view) reveals that the easy axis of the magnetization $M_{||}$ is at $\Phi = -90^\circ$ (perpendicular to the Cu step edges) for 1 ML Fe on 11 ML Ni. For 2.9 ML Fe the easy axis is at $\Phi = -16^\circ$, i. e. along [001]. The in-plane component of $\mathbf{M}$ rotates from "perpendicular to the steps" into the [001] direction by crossing the SRT. This in-plane rotation was observed for both Ni thicknesses. Since the steps do not run

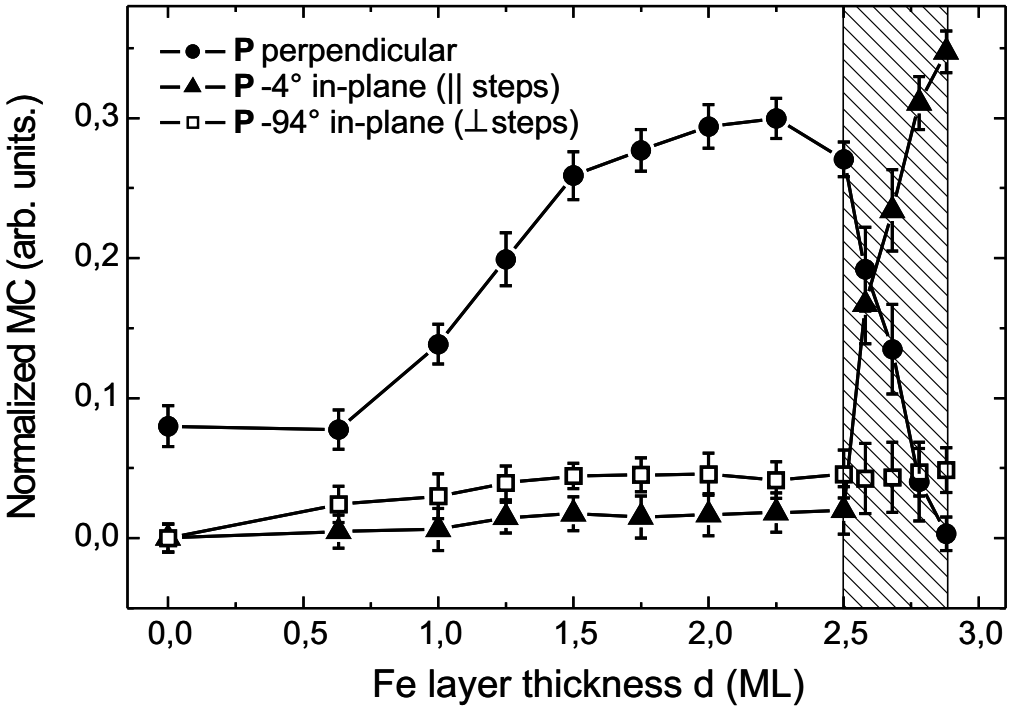

Figure 6.9: Angular dependent normalized magnetic contrast versus the Fe layer thickness x of an Fe_x/Ni_{11}/Cu(100) film at 300 K. The hatched area demonstrates the interval of the SRT. Below 2.5 ML Fe the perpendicular component of the magnetization $\mathbf{M}$ increases (–●–) while the two in-plane components stay almost constant. The in-plane components are much smaller and point into directions of $\Phi = -4°$ (–▲–) and $\Phi = -94°$ (–□–) with respect to the Cu step edges. Note that the in-plane MC perpendicular to the steps (–□–) occurs around 0.6 ML Fe before a component of $\mathbf{M}$ parallel to the steps is established. During the SRT the magnetization direction switches from out-of-plane to in-plane, while the in-plane component rotates from normal to almost parallel to the steps.

parallel to a crystallographic axis, the "perpendicular to the steps" orientation of the in-plane component of $\mathbf{M}$ has to be interpreted in terms of a step-induced anisotropy perpendicular to the steps. The in-plane component of the canted magnetization of the 7 ML Ni/Cu(100) *without* the Fe top layer showed the same orientation perpendicular to the Cu step edges. This indicates that the in-plane preferential direction "perpendicular to the steps" is not due to the Fe layer, but it originates either directly from the Cu steps or from an interplay between the magnetic anisotropy, induced by the step edges and the bulk magnetoelastic contribution of the Ni film. The latter favors an easy axis perpendicular to the surface and, thus, at least to some degree also perpendicular to the step edges. At larger Fe thicknesses, the in-plane anisotropy of Fe dominates, which then favors the [001] direction.

Fig. 6.9 shows the magnetic contrast, normalized to the background grayscale, as obtained from the individual domain images taken at three different directions of $\mathbf{P}$ (see Fig. 6.7) as a

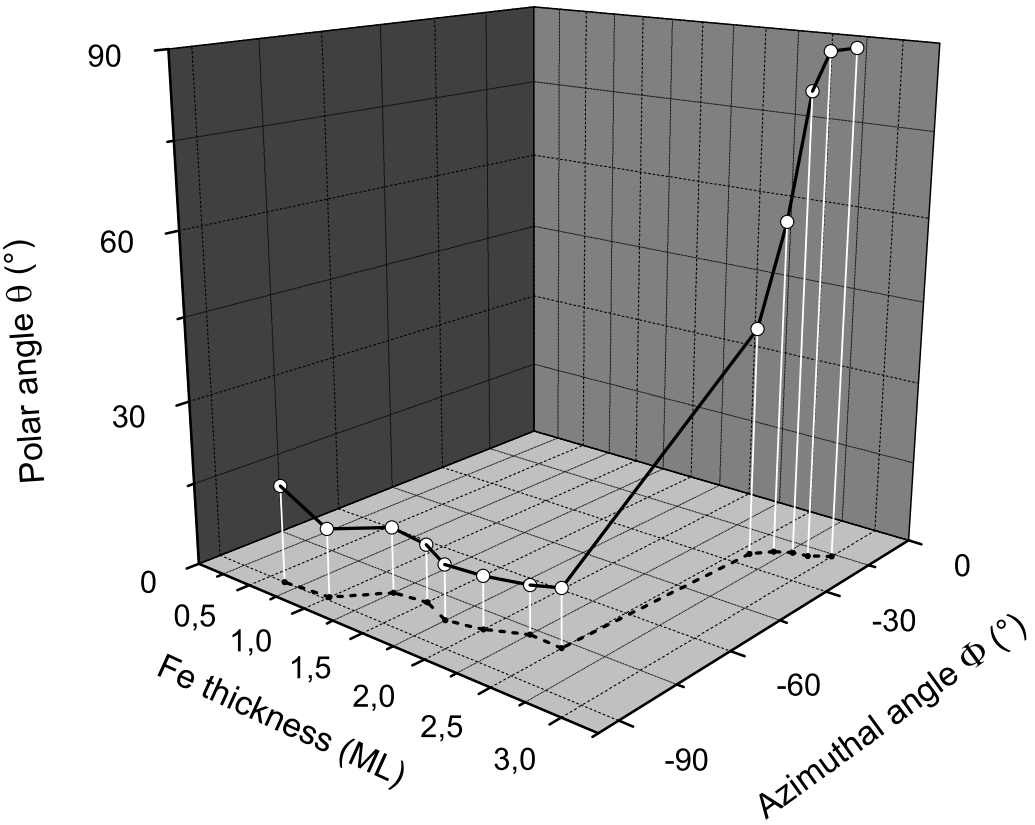

Figure 6.10: 3D-plot of the angular dependence of the magnetization direction versus the Fe layer thickness x of an $Fe_x/Ni_{11}/Cu(100)$ film at the spin-reorientation transition at 300 K. θ is the angle between the surface normal and the easy axis of the in-plane component of the magnetization. It is derived from a series of SPLEEM images, which are partly shown in Fig. 6.7. Φ is the azimuthal angle measured counter-clockwise against the direction of the substrate steps (see Fig. 6.7).

function of the Fe layer thickness. The in-plane contrast obtained for $\Phi = -4°$ remains small and constant up to 2.5 ML Fe, where it sharply increases upon reaching the SRT. At around 0.6 ML Fe, a small MC occurs for the $\Phi = -94°$ direction, which then stays constant within error limits up to 2.9 ML Fe. The behavior of the perpendicular component may be divided into 4 thickness ranges: Below 0.6 ML Fe, the MC is constant, followed by two intervals, where the MC strongly ($0.6 - 1.5$ ML Fe) and weakly ($1.5 - 2.25$ ML Fe) increases. Finally, a rather strong drop to zero of the MC is observed within the SRT interval from 2.5 to 2.9 ML Fe.

The observed plateau in the perpendicular MC below 0.6 ML Fe can be explained as resulting from two effects, namely from a reduced magnetic moment per Fe atom on the Ni surface, and from the canting of the magnetization. Obviously, the expected increase of the MC following the increasing number of Fe magnetic moments is here compensated by a respective reduction of the perpendicular magnetization component due to the canting angle of $\theta \approx 17°$ found for the case of $\Phi = -94°$. This canting angle reduces the normal component of M by

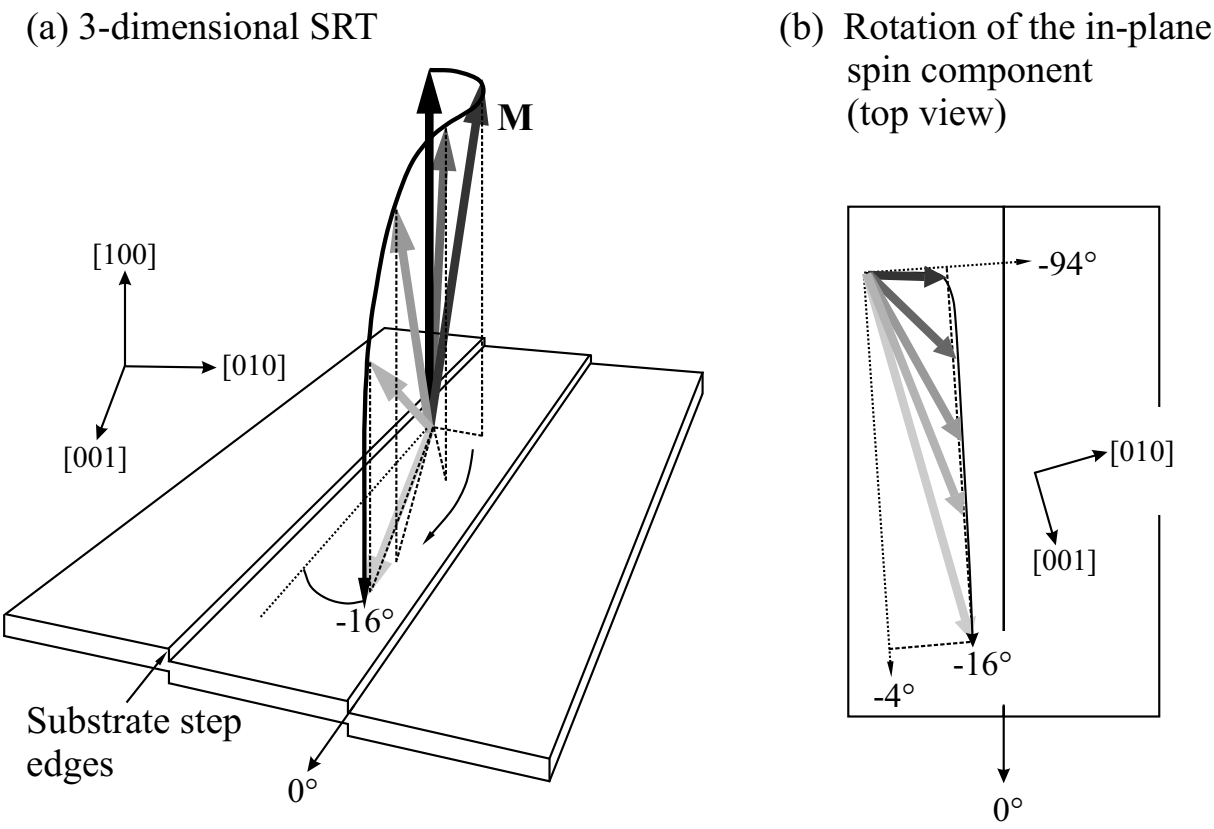

Figure 6.11: Model of the spiral-like motion of the magnetization vector of Fe/Ni/Cu(100) films during the spin-reorientation transition. The perpendicular magnetization **M** spontaneously tilts off the [100] direction with the in-plane component normal to the Cu step edges at the beginning of the SRT and rotates into the [001] in-plane direction at the end of the SRT (a). The brightness of the magnetization vectors scales with increasing Fe layer thickness. The accompanied rotation of the in-plane component of **M** is sketched in (b).

≈4.4%, which exactly compensates the increase of the average magnetic moment within error bars. One might also speculate that at the Fe layer of 0.6 ML the Fe atoms do not carry their usual bulk magnetic moment, but that the Fe moment is reduced within the Fe/Ni interface due to alloy formation. If one assumes the bulk magnetic moments of 2.2 μ_B and 0.62 μ_B per Fe and Ni atom, respectively, the average moment of the Fe/Ni bilayer would increase by 13%. In order to compensate for the according increase in magnetic contrast, a canting angle of ≈30° would be required, which almost doubles the measured canting angle. On the other hand, from the measured canting angle of 17°, a magnetic moment of ≈1.1 μ_B is obtained for Fe, which is unrealistic at first glance. However, the angle θ as obtained from SPLEEM images inhibits an uncertainty of $\pm 5°$, such that the magnetic moment as obtained in the case of weak MC is just a rough estimate. On the other hand, element-specific XMCD measurements (section 6.2.2) reveal, that the magnetic moment of 1 ML Fe on 17 ML Ni/Cu(100) is indeed reduced to a value of ≈1.7 μ_B at 300 K, which supports the reduced Fe moment derived from the domain images.

Fig. 6.10 shows (in a 3-dimensional plot) the superposition of the polar angle θ, measured between the surface normal and the easy axis of the in-plane component of $\mathbf{M}$, and the azimuthal angle Φ, both as a function of the Fe layer thickness. Below 2.5 ML Fe the polar angle remains at $\theta = 13^\circ \pm 5^\circ$, whereas the azimuthal angle changes from "perpendicular to the steps" ($\Phi = -90^\circ$) to $\Phi \approx -77^\circ \pm 5^\circ$. At 2.5 ML Fe the SRT starts with a breakup of the original domains, and both the polar and the azimuthal angle vary drastically. The in-plane component of $\mathbf{M}$ performs a rotation of $\Phi \approx 50^\circ$ within a range of the Fe thickness of less than 0.1 ML. Within the same interval, θ increases by almost 40°. A further rotation of $\Delta\theta \approx 40^\circ$ occurs for the Fe thickness ranging from 2.6 to 2.9 ML. Here, Φ further changes by only ≈6°, such that the magnetization is finally oriented parallel to the [001] easy direction.

The spiral-like SRT that is discovered at least qualitatively by the series of domain images is additionally illustrated in Fig. 6.11 (a) as a three dimensional sketch, which shows the superposition of the spin-reorientation from out-of-plane to in-plane. The top view (Fig. 6.11 (b)) shows the rotation of only the in-plane component, starting from "perpendicular to the Cu step edges" to the easy axis of the magnetization, which is the [001] direction. In order to comply with the information obtained from the series of domain images, in our model of the SRT the projection of $\mathbf{M}$ onto the $\Phi = -94^\circ$ direction is kept constant, as shown in Fig. 6.7 (b). Thus, in Fig. 6.11 the arrowheads of the in-plane magnetization vectors follow a slight curve, which then allows for an equal projection onto the $\Phi = -94^\circ$ direction. This, then nicely explains the unchanged magnetic contrast as measured in that orientation.

6.2.4 Determination of the Fe-Ni interface magnetic anisotropy from the critical Fe layer thickness

The domain images at 300 K unambiguously reveal that the reorientation of the magnetization is a continuous one. To describe the nature of a continuous SRT, the magnetic anisotropy constants of second and fourth-order have to be included in the consideration [3]. First of all, the orientation of the magnetization of the Fe/Ni bilayer is determined by the delicate balance between the intrinsic magnetic anisotropy energy (MAE) and the shape anisotropy. As stated before in section 1.2.1 the shape anisotropy always favors an in-plane orientation of $\mathbf{M}$, whereas the intrinsic MAE may either favor an in-plane or a perpendicular orientation of $\mathbf{M}$, which is expressed in terms of the ratio of the respective anisotropy constants. The observed SRT from an out-of-plane to an in-plane direction occurs, when the shape anisotropy dominates over the magnetocrystalline anisotropy upon the increase of the Fe layer thickness. The easy axis of the magnetization is determined by the minimum of the free energy density F per unit area, which in

the case of the tetragonal bilayer system Fe/Ni on Cu(100) includes the following contributions:

$$\begin{aligned} F &= \left(\frac{1}{2}\mu_0 M_{Ni}^2 - K_{2,Ni}^V\right)\cos^2\theta\, d_{Ni} + \left(\frac{1}{2}\mu_0 M_{Fe}^2 - K_{2,Fe}^V\right)\cos^2\theta\, d_{Fe} - K_2^{S,\text{eff}}\ \cos^2\theta - \\ &\quad -\frac{1}{2}K_{4\perp}^{\text{eff}}\ \cos^4\theta - \frac{1}{8}K_{4\parallel}^{\text{eff}}\ (3+\cos 4\Phi)\sin^4\theta - J\ \mathbf{M}_{Ni}\cdot\mathbf{M}_{Fe} \end{aligned} \tag{6.1}$$

where $K_2^{S,\text{eff}} = K_{2,Ni-Cu}^S + K_{2,Fe-Ni}^S + K_{2,Fe-vac}^S$ and
$K_i^{\text{eff}} = K_{i,Ni}^V\, d_{Ni} + K_{i,Fe}^V\, d_{Fe} + K_{i,Ni-Cu}^S + K_{i,Fe-Ni}^S + K_{i,Fe-vac}^S$ with $i = 4\perp,\ 4\parallel$. θ is the polar angle with respect to the [100] direction, Φ is the azimuthal angle measured against the easy [001] in-plane direction of the system. J is the ferromagnetic coupling constant between the magnetizations M_{Ni} and M_{Fe} of Ni and Fe, which are always aligned parallel as shown by the XMCD measurements in section 6.2.1. K_2, $K_{4\perp}$ and $K_{4\parallel}$ are the second- and the fourth-order perpendicular and in-plane terms of the MAE. K^V denotes the volume contribution and K^S the various surface- and interface anisotropies as given by the lower index. If $K_{4\perp} = K_{4\parallel} = 0$, no tilted orientation of the magnetization is possible. Hence, if K_2 changes, a *discontinuous* reversal of the magnetization is expected [22]. Since we observe both an out-of-plane spin-canting as well as a continuous rotation of the magnetization, the second-order contributions to the MAE alone are not sufficient to account for this behavior. Thus, a fourth-order contribution needs to be included within the analysis. However, the reorientation interval of 0.4 ML Fe is rather small, i. e. the K_4 values are also small. For this reason the K_4 values are neglected in the further analysis. Only if $K_4 \gg K_2$, the difference between the critical thicknesses d_{c1} and d_{c2}, which denote for the onset and the end of the SRT, becomes significant. It should be noted, though, that SPLEEM is a suitable technique, in order to reveal even such a small difference between the lower and the upper critical thickness, which then makes it feasible to determine the true nature of this transition. In the following approximation we consider the 0.4 ML interval as a discontinuous reversal of $\mathbf{M}$ at a mean value $d_{c,Fe} = 2.7$ ML .

In our simplified model, the sum of the shape anisotropy and the crystalline anisotropy contributions vanishes at $d_{c,Fe}$:

$$\begin{aligned} \left(\frac{1}{2}\mu_0 M_{Ni}^2 - K_{2,Ni}^V\right)d_{Ni} + \left(\frac{1}{2}\mu_0 M_{Fe}^2 - K_{2,Fe}^V\right)d_{Fe} - K_{2,Ni-Cu}^S - K_{2,Fe-Ni}^S - \\ -K_{2,Fe-vac}^S = 0. \end{aligned} \tag{6.2}$$

For the following discussion of the question, which of the various contributions plays the major role for the observed SRT, we consider two scenarios. In the first case, a sharp interface between the Fe and Ni layer is assumed and the volume, interface and surface contributions for Fe and Ni layers on Cu(100) are taken from the literature (table 6.3). The shape anisotropy of the bilayer structure here increases from 7.5 μeV/atom [9] to 32 μeV/atom (averaged for the bilayer) by the deposition of Fe, due to the 3.5 times larger bulk magnetic moment of the Fe atoms (2.22 μ_B) as compared to the Ni atoms (0.62 μ_B). Using these values together with the literature values of

Table 6.3: Anisotropy constants of Ni/Cu(100) and Fe/Cu(100) at 300 K.

Anisotropy constant	Energy (μeV/atom)	Reference
$K^V_{2,Ni}$	30	[37]
$K^V_{2,Fe}$	77.7	[199]
$K^S_{2,Ni-Cu}$	-59	[83]
$K^V_{2,Fe-vac}$	64	[31]

the anisotropy constants listed in table 6.3, one realizes, that the sum of these quantities is zero, only, if an interface anisotropy $K^S_{2,Fe-Ni} = -93$ μeV/atom is present. Thus, a *large negative interface anisotropy* is needed to explain the critical thickness of 2.7 ± 0.2 ML for the SRT. Note, that in the case of Fe/Cu(100), where no Fe-Ni interface is present, the magnetization of 3 ML Fe grown at 300 K is oriented perpendicular to the surface [169].

In a second but more realistic approach we consider intermixing within the interface, which then may result in an $Fe_{0.5}Ni_{0.5}$ alloy spanning over two monolayers. According to the Slater-Pauling curve, the average magnetic moment per atom in these two layers is $\approx$1.6 μ_B. Recalculation of the shape anisotropy of the Fe/Ni bilayer with a 2 ML thick alloyed interface region, but keeping constant the number of deposited Fe and Ni atoms, and assuming an enhanced magnetic moment of the 1.7 ML thick toplayer of 2.7 μ_B, yields an increase of the shape anisotropy by only about 15%. Thus, we can conclude that the increase of the shape anisotropy as a function of the Fe thickness is not sufficient to force the direction of the magnetization of the bilayer into the film plane below a thickness of 3 ML Fe. A relatively large Fe-Ni interface anisotropy needs to be taken into account to explain the critical Fe thickness at which the SRT occurs.

Determination of an effective fourth-order anisotropy constant

The SPLEEM images prove that the SRT is a continuous one over a *small* thickness interval. As mentioned above, the value of K_4 is therefore expected to be small. The analysis of the polar angle θ as a function of the Fe layer thickness allows for a rough estimation of the effective anisotropy coefficient K_4^{eff}, which represents the average of the fourth-order contributions of the entire bilayer. In Fig. 6.12 the polar angle is displayed as a function of the Fe thickness within an interval of 2.25 ML to 3.0 ML. The solid line is a fit based on the minimization of the free energy density per unit area given by Eq. (6.1) with respect to θ. For simplicity, a cubic lattice is assumed, i. e. $K_{4\perp} = K_{4\parallel} = K_4^{\text{eff}}$. The unit of K_4^{eff} is "energy per volume" due to the separation $K_4^{\text{eff}} = K_4^{V,\text{eff}} + K_4^{S,\text{eff}}/d$. In a strict sense the Fe and the Ni layers contribute to both $K_4^{V,\text{eff}}$ and $K_4^{S,\text{eff}}/d$. However, measurements by ferromagnetic resonance (FMR) yield values of K_4^V for Ni/Cu(001) that are more than three times smaller than the K_4^S constants [22].

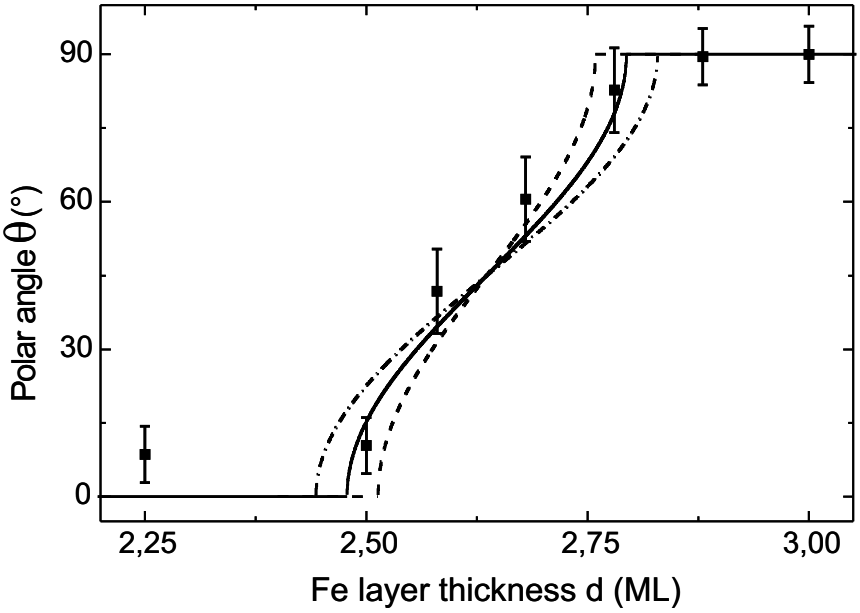

Figure 6.12: Angular dependence of the magnetization direction versus the Fe layer thickness x of an Fe_x/Ni_{11}/Cu(100) film at the spin-reorientation transition at 300 K. θ is the angle between the surface normal and the magnetization vector, which is derived from a series of domain images which in part is depicted in Fig. 6.7. The curves represents the fits according to Eq. (6.4). For details see text.

Moreover, due to the small layer thickness of Fe the volume contribution to $K_4^{V,\text{eff}}$ from the Fe layer is regarded as negligible. Hence, $K_4^{V,\text{eff}}$ is neglected in the following, i. e. K_4^{eff} will be treated as a pure surface/interface contribution of the bilayer.

Minimization of the free energy density per unit area (Eq. 6.1) for the case $K_{4\perp} = K_{4\parallel} = K_4^{\text{eff}}$ and $\Phi = 0$, yields $\theta = 0°$ and $\theta = 90°$, which correspond to the orientation of the magnetization before and after the SRT, respectively, and:

$$\cos^2\theta = \left(\left(\frac{1}{2}\mu_0 M_{Ni}^2 - K_{2,Ni}^V\right) d_{Ni} + \left(\frac{1}{2}\mu_0 M_{Fe}^2 - K_{2,Fe}^V\right) d_{Fe} - K_{2,Ni-Cu}^S - K_{2,Fe-Ni}^S - K_{2,Fe-vac}^S + K_4^{\text{eff}}\right) / \left(2K_4^{\text{eff}}\right). \quad (6.3)$$

within the reorientation interval. The solid, dashed and dashed-dotted lines in Fig. 6.12 are given by

$$\theta = \arccos\sqrt{\left(\left(\frac{1}{2}\mu_0 M_{Ni}^2 - K_{2,Ni}^V\right) d_{Ni} + \left(\frac{1}{2}\mu_0 M_{Fe}^2 - K_{2,Fe}^V\right) d_{Fe} - K_{2,Ni-Cu}^S - K_{2,Fe-Ni}^S - K_{2,Fe-vac}^S + K_4^{\text{eff}}\right) / \left(2K_4^{\text{eff}}\right)}. \quad (6.4)$$

for different values of K_4^{eff}. The error bars in Fig. 6.12 identify the individual inaccuracy in the determination of the polar angle from each domain image. Error bars range from $\pm 5°$ for the large out-of-plane and in-plane domains with reasonable magnetic contrast to $\pm 8°$ for the

case of stripe domains. The fit yields an interval of less than 0.3 ML for the width of the spin-reorientation transition.

In order to determine K_4^{eff} from this fit, the anisotropy constants of Ni/Cu(100) and Fe/Cu(100) from table 6.3 were used. A saturation magnetization of Fe of 1820 kA/m, which is ≈4.5% enhanced with respect to the literature value for bulk bcc Fe, was taken to account for the increased average magnetic moment found by XMCD measurements for an Fe coverage of 4 ML. Since $K^S_{2,Fe-Ni} = -93$ μeV/atom was determined, provided that $K_4^{\text{eff}} = 0$, i. e. assuming a discontinuous SRT at 2.7 ML Fe, both $K^S_{2,Fe-Ni}$ and K_4^{eff} were varied. The fit, which is given by the solid line in Fig. 6.12, yields $K^S_{2,Fe-Ni} = -68$ μeV/atom and $K_4^{\text{eff}} = -10.7$ μeV/atom. The value for K_4^{eff} is of reasonable magnitude compared to the second-order coefficients. Although the error of the determined K_4^{eff} is expected to be too large to make the value of K_4^{eff} comparable to anisotropy constants determined by other methods like FMR, the existence of a non-zero K_4^{eff} is all-important to fit the data points in Fig. 6.12, which correspond to canted magnetization vectors. For comparison, another two fits are shown in the figure, which yield $K_4^{\text{eff}} = -13.0$ μeV/atom (dashed line) and $K_4^{\text{eff}} = -8.3$ μeV/atom (dashed-dotted line) for the same value of $K^S_{2,Fe-Ni}$. Note also that K_4^{eff} is negative in all three cases. This means, that also the numerator in the square root of Eq. (6.4) must be negative in the Fe thickness range from 2.5 to 2.9 ML, such that the radicand remains positive. Thus, according to $\tilde{K}_2 = K_2 - \frac{1}{2}\mu_0 M^2$, (see Fig. 1.4), $\tilde{K}_2$ must be positive for the Fe/Ni bilayer system. Then, the SRT takes place in the fourth quadrant of the anisotropy diagram (Fig. (1.4)), for which theory [4,11] predicts a canted magnetization in agreement with our results. Interestingly, the breakup of the large domains into stripe domains of a cosine-like profile, which is theoretically predicted to occur in the *second* quadrant at positive K_4 and negative $\tilde{K}_2$ values, is *simultaneously* observed during the reorientation process.

6.2.5 Domain wall evolution near the SRT

The same reorientation behavior of the magnetization is found for Fe/Ni bilayers, when Fe is deposited on an 11 ML Ni/Cu(100) underlayer and a 7 ML Ni/Cu(100) underlayer. The latter one is in a state of a canted magnetization with the in-plane component of the magnetization oriented perpendicular to the Cu step edges. Again, there is no magnetic contrast detected in the $\Phi = -4°$ polarization orientation for Fe coverages below 1 ML but in the $\Phi = -94°$ direction. The MC remains nearly constant in the $\Phi = -94°$ direction, whereas the MC in the $\Phi = -4°$ direction increases only weakly up to an Fe coverage of 2.5 ML, followed by a dramatic increase just at the thickness, where the domains break up into stripes. The orientation of the magnetization within the in-plane domains after crossing the SRT is again directed along [001], confirming a similar spiral-like magnetization reorientation as it was found for the bilayer with 11 ML Ni. Fig. 6.13 shows a domain wall of the Fe_x/Ni_7 bilayer imaged with $\mathbf{P}$ oriented

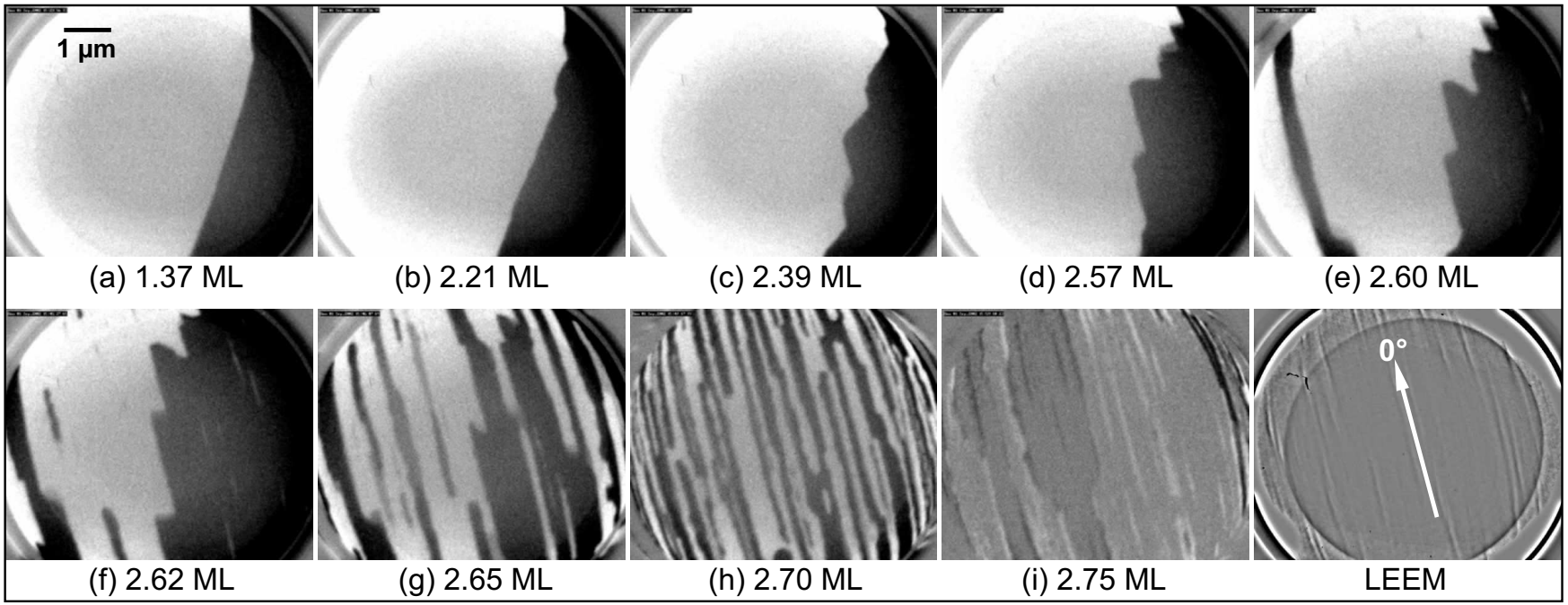

Figure 6.13: Domain wall evolution as a function of the Fe layer thickness (a)-(i) on a 7 ML Ni/Cu(100) film at 300 K imaged with the polarization **P** of the electron beam directed normal to the surface. Stripe domains evolve from the original straight domain wall. The stripe domains are parallel to the Cu atomic step edges (0°), which is confirmed by the LEEM image of the bare Cu(100) surface. The low magnetic contrast in (i) indicates that the magnetization has almost completely rotated into the film plane.

perpendicular to the surface as a function of Fe deposition. The direction of the wall segment was found to have no correlation with topographic features, as can be seen by comparing the magnetic SPLEEM images with the LEEM image of the bare Cu crystal surface. At about 1.4 ML Fe the observed domain wall is almost straight, but it is not pinned to the substrate. Note also, that there is just one domain wall within the 7 μm-field of view (Fig. 6.13 (a)). Both latter facts indicate, that the domain wall energy must be relatively high. As the Fe layer thickness increases, the domain wall starts to extend by forming protrusions, similar to that of the domain wall at the SRT of Ni/Cu(100). Here, however, the domain wall starts to adjust to the substrate step edges by forming rectangular protrusions with one side running parallel to the direction of the Cu atomic steps (6.13 (b)-(c)). Obviously, lowering of the effective anisotropy due to the Fe deposition is responsible for the elongation of the domain wall, following a reduced wall energy according to $\gamma \propto d\sqrt{A\,K_2^{\text{eff}}}$. The alignment of wall segments with the step edges further minimizes the wall energy. Finally, this process evolves into a stripe domain pattern along the step direction (6.13 (e)). At about 2.6 ML Fe (6.13 (c)) stripe domains along the steps also appear spontaneously somewhere within the domains. The average stripe domain width at the maximum number of stripes around 2.7 ML Fe is about 180 nm, which is comparable to the wall width measured for 2.2 ML Fe/Cu(100).

The detailed analysis of domain walls in out-of-plane magnetized Fe/Ni bilayers has shown that the walls are Bloch walls (section 5.3.1), whereas in in-plane magnetized Fe/Ni bilayers the walls are of Néel type (section 5.3.2). Obviously, there is a transition from Bloch type to Néel type domain walls during the SRT from out-of-plane to in-plane. In Fig. 6.14 such a transition is typically demonstrated for an $\text{Fe}_x/\text{Ni}_7/\text{Cu}(100)$ film as a function of the Fe layer thickness x. At the start of the SRT at 2.6 ML Fe, the black and white MC of the domain walls in the image with $\mathbf{P}$ directed along the $\Phi = -4^\circ$ in-plane direction (a_1) and the zero MC perpendicular to that direction in the film plane (b_1) clearly shows, that the walls are Bloch walls. At the breakup into a multi stripe domain pattern at 2.7 ML Fe most of the domain walls are in a transition state between the Bloch and the Néel mode, which is indicated by the SPLEEM images (a_2), (b_2) and their corresponding modified images (a_3), (b_3), where areas of zero MC are enhanced. In these two images the domain walls are identified from both orientations of $\mathbf{P}$, which confirms that the magnetization within the wall consists of both in-plane components. The domain images probing the component of $\mathbf{M}$ normal to the surface (not shown) confirm that the magnetization within the walls rotates in the plane. The white and black arrows in the images indicate the identical features. A close inspection of these spots reveals, that a few wall segments are still in the Bloch mode, whereas others are already in the Néel mode.

After completion of the SRT at 2.8 ML Fe, all domain walls are Néel walls (Fig. 6.14 (a_4), (b_4)), i. e. the orientation of the magnetization within the wall has rotated by 90° within the plane into the Néel wall mode during the SRT. The slight shift of the walls in (a_4), (b_4) is due to

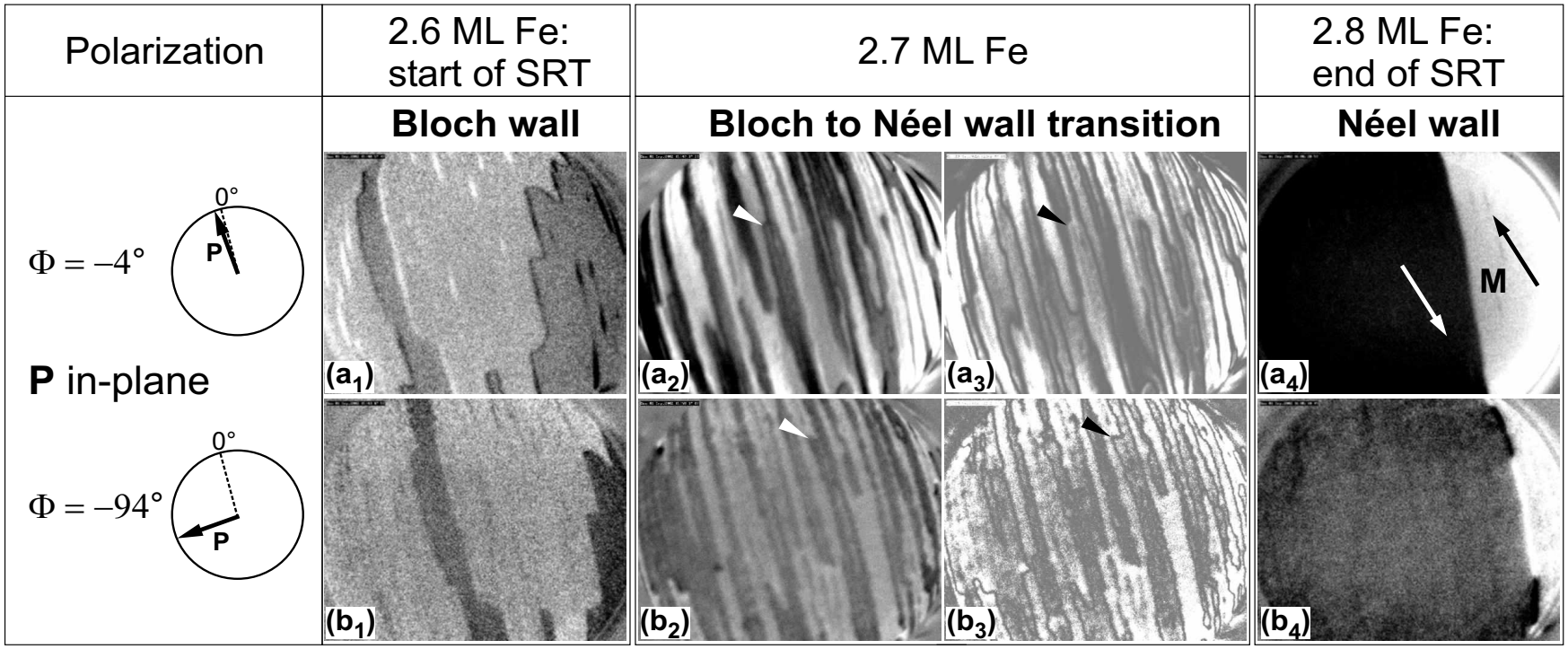

Figure 6.14: Bloch to Néel wall transition of an $Fe_x/Ni_7/Cu(100)$ film as a function of the Fe layer thickness x during the SRT at 300 K. Left: After the start of the SRT at 2.6 ML Fe the black domain wall is identified as a Bloch wall with the magnetization rotating collinear to the $\Phi = -4°$ direction (a_1, no MC of the wall in b_1). At the breakup into stripe domains (2.7 ML Fe) most of the domain walls are in a transition state between the Bloch and Néel mode, which is indicated by the SPLEEM images (a_2), (b_2) and their corresponding modified images (a_3), (b_3), where areas of zero MC are enhanced. The domain walls are revealed in both orientations of $\mathbf{P}$, confirming that the magnetization in the wall has both in-plane components. The white and black arrows show the same feature. Right: At the end of the SRT the domains are in-plane magnetized. The orientation of the magnetization within the wall has rotated by 90° within the plane into the Néel wall mode (a_4, b_4). The shift of the wall is due to a misalignment between the polarization directions.

a misalignment between the polarization directions. The direction of the magnetization within the domains was determined from an image, where $\mathbf{P}$ was oriented in-plane at $\Phi = -106°$ away from the direction of the step edges, in which the MC between the domains vanishes. Consequently, $\Phi = -16°$, i. e. the [001] direction, is the easy axis of the magnetization like in the Fe/Ni bilayer with 11 ML Ni.

6.2.6 SRT of Fe_x/$Ni_{1.5}$/Cu(100)

In contrast to the investigations of the SRT of Fe/Ni bilayers containing a Ni/Cu(100) film, which exhibits an out-of-plane magnetization, the domain formation at the SRT of Fe grown on 1.5 ML Ni/Cu(100) is presented in the following. According to the magnetic phase diagram shown in Fig. 1.7, 1.5 ML Ni on Cu(100) is in the paramagnetic state at room temperature. This is confirmed by the domain images, which do not reveal any magnetic contrast perpendicular or parallel to the surface (not shown). Upon Fe deposition on top of the Ni film the formation of $\approx 1-2$ μm wide stripe domains occur at 1.35 ML Fe. Both a perpendicular and an in-plane component of the magnetization within the domains is detected, which is depicted in Fig. 6.15 and indicates a canted magnetization. The canting angle with respect to the surface normal derived from the SPLEEM images is $\theta \approx 30°$. Two clear differences of the domain formation at the onset of ferromagnetism at 300 K of the Fe/Ni/Cu(100) film as compared to the Fe/Cu(100) film, which was previously grown on the same substrate can be pointed out: (i) the domain width is considerably larger and (ii) the magnetization is canted as domains occur in the Fe/Ni bilayer. Firstly, the high density of perpendicularly magnetized stripe domains of Fe/Cu(100) at 2.2 ML was explained by the reduction of the stray field energy, which is large due to the large magnetic moment of Fe. Furthermore, the ratio of the magnetocrystalline anisotropy to the shape anisotropy near unity characterized the pure cosine-like domain profile (section 5.2). In the bilayer system only 1.35 ML Fe and 1.5 ML Ni, which are most likely alloyed, contribute to the magnetic stray field. The individual magnetic moments of Fe and Ni near an $Fe_{0.5}Ni_{0.5}$ alloy have been determined to reach values of 2.5 μ_B and 0.7 μ_B [46], respectively, which yields a thickness-weighted average magnetic moment of about 1.6 μ_B in agreement with the Slater-Pauling curve. On the other hand high-spin states of tetragonally distorted Fe monolayers on Cu(100) with moments up to 3.55 μ_B have been reported [198]. Consequently, the stray field energy of the considered bilayer is smaller than that of the Fe/Cu(100) film of 2.2 ML thickness and can be reduced by a smaller number of larger domains. Secondly, the canted magnetization, which is found in all Fe/Ni/Cu(100) films studied in this work, indicates that the Fe-Ni interface anisotropy is negative and thus shifts the anisotropy balance in favor of an in-plane orientation of the magnetization. Eventually, the ratio of the reduced perpendicular anisotropy to the small shape anisotropy of the $Fe_{1.35}$/$Ni_{1.5}$/Cu(100) must be larger than that of Fe/Cu(100) in order to stabilize the observed broad stripe domains.

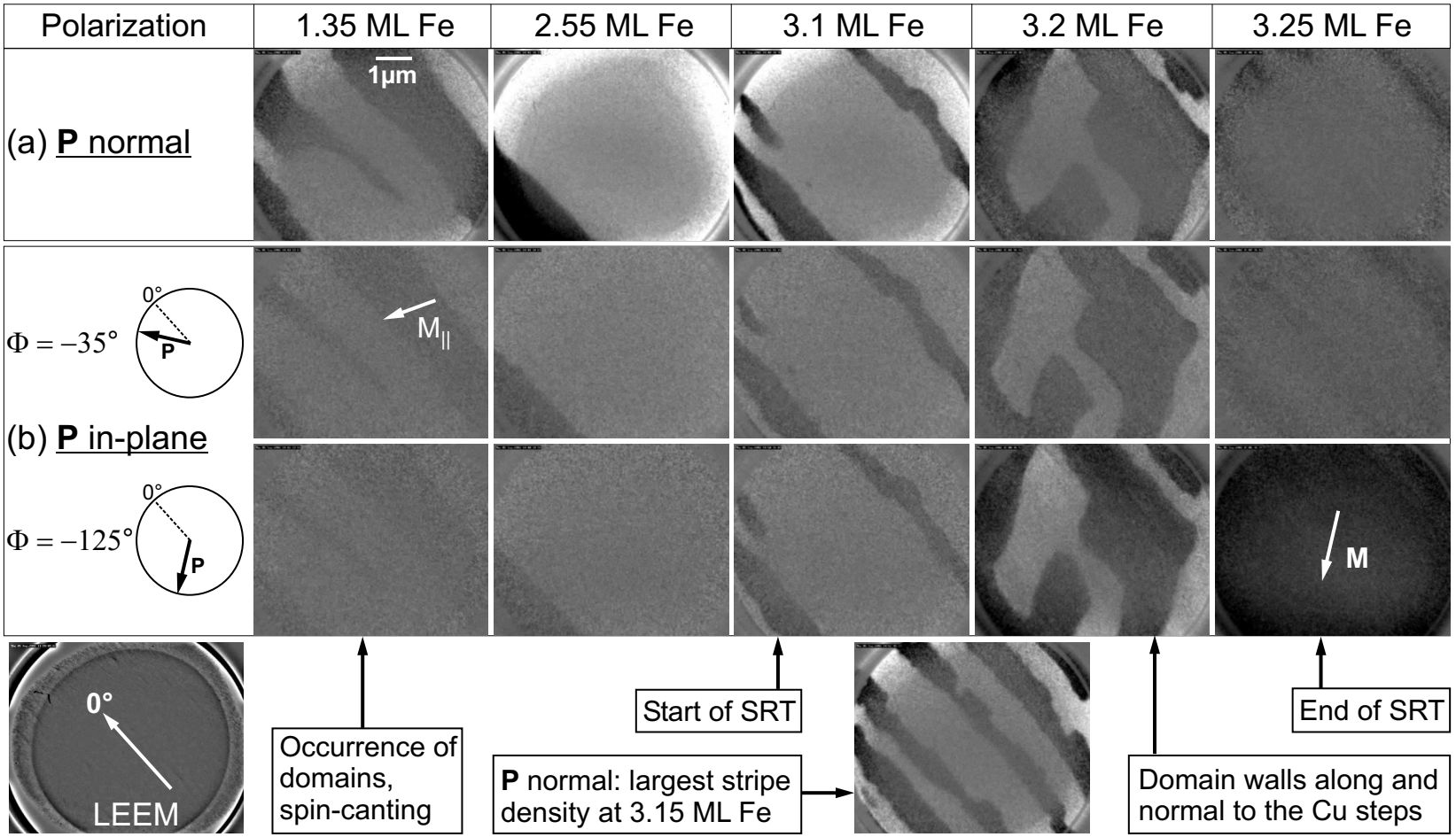

Figure 6.15: Domain formation of an $Fe_x/Ni_{1.5}/Cu(100)$ film at the SRT. At 1.35 ML Fe $1-2$ μm wide magnetic stripe domains, aligned with the Cu step edges, occur, in which the magnetization is canted. The domains laterally expand up to 3.1 ML Fe, where the SRT starts via a breakup into ≈750 nm wide stripes. A domain pattern with domain walls oriented both parallel and perpendicular to the Cu steps forms as the magnetization continuously rotates into the film plane.

As the Fe thickness grows further the domains become larger in agreement with the observation of Fe on thicker Ni/Cu(100) films and previous findings [105,106]. The size of the domains reaches its maximum of more than 7 μm around 3 ML Fe. Also in Fe/Cu(100) films the largest domains form around 3 ML, but the average width is on the order of only 2 μm. At 3.1 ML Fe the SRT of the bilayer starts via a disintegration into a stripe domain pattern. As compared to the stripe formation observed for Fe monolayers on 7 ML and 11 ML Ni two differences arise: (i) the critical thickness for the breakup into stripe domains is shifted to a larger Fe thickness by 0.6 ML and (ii) the width of the stripe domains at the highest density of stripes is ≈750 nm for the $Fe_{1.35}/Ni_{1.5}$/Cu(100) film, which is more than four times larger. This finding may again be attributed to the smaller magnetic stray field of the bilayer due to the minor Ni layer thickness. Besides the quantitative differences, as compared to bilayers containing thicker Ni layers (sections 6.2.3-6.2.5) the formation of domains up to the stripe pattern are qualitatively similar in both systems. However, a unique domain pattern of the $Fe_{1.35}/Ni_{1.5}$/Cu(100) film is observed at 3.2 ML Fe, as the in-plane component of the magnetization starts to rotate towards the $\Phi = -125^\circ$ direction where the domain size increases again. These domains are separated by domain boundaries running partially along and almost perpendicular to the substrate step edges, respectively, and thus forming rectangular corners. No such behavior was found in other Fe/Ni bilayers. At the end of the SRT at 3.25 ML Fe the magnetization lies in the film plane with its easy axis parallel to the $\Phi = -125^\circ$ direction, which is confirmed by the vanishing contrast in the domain images, which detect the perpendicular and the in-plane component with $\mathbf{P}$ along the $\Phi = -35^\circ$ direction in Fig. 6.15. The thickness interval of the SRT is about 0.15 ML Fe, which is less than half the value found for bilayers with thicker Ni layers. Despite this small value the magnetization reorientation is unambiguously demonstrated to be a transition of second order by the spin canting within the domains. The smaller reorientation interval must be interpreted in terms of smaller anisotropy contributions of second and fourth order. In particular the volume part of the magnetocrystalline anisotropy of Ni is considered to be negligible due to the small amount of Ni.

In the present case neither at the start nor at the end of the SRT the in-plane component of the magnetization coincides with the Cu step direction. In summary, a spiral-like continuous SRT is found in $Fe_{1.35}/Ni_{1.5}$/Cu(100) films, which is in qualitative agreement with the other Fe/Ni films studied in this work. However, the SRT starts at an increased Fe thickness and a unique domain pattern is revealed compared to the other bilayer systems. The differences of the domain formation of ultrathin Fe layers grown on Cu(100) have been elaborated, which emphasize the strong influence of alloying at the Ni/Fe interface.